Coupled Analysis Method for High-Field Magnet Coil using Coated Conductor Based on J-E Characteristics as a Function of Temperature, Magnetic Field Vector and Mechanical Stain

Coupled Analysis Method for High-Field Magnet Coil Using Coated Conductor Based on J-E Characteristics as a Function of Temperature, Magnetic Field Vector and Mechanical Strain

Kohei Higashikawa, Takanobu Kiss, Masayoshi Inoue, Kazutaka Imamura, Taketsune Nakamura, Satoshi Awaji, Kazuo Watanabe, Hiroyuki Fukushima, Yutaka Yamada, and Yuh Shiohara

***Abstract*—We have characterized nonlinear current transport properties in a coated conductor as a function of temperature, magnetic field vector and mechanical strain, and then have developed a thermally-electromagnetically-structurally coupled analysis code for a high-field magnet coil. The distributions of heat generation and electromagnetic force in the coil are computed by electromagnetic analysis. Then, the temperature distribution and the strain distribution are correspondingly calculated by thermal analysis and by structural analysis. Furthermore, both of them are fed back to the electromagnetic analysis. These analyses are based on finite element method, and are repeated until the convergence. By taking a design example of a 40 T class magnet coil using a GdBCO coated conductor, we have discussed the necessity of the consideration of thermally-structurally influenced transport properties in the coil for the coil design.**

***Index Terms*—Coupled analysis, finite element method, GdBCO coated conductor, high-field magnet, HTS coil.**

I. Introduction

THE second-generation high temperature superconducting (HTS) wires such as REBCO (RE: Y, Gd and so on) coated conductor (CC) has been steadily developed in recent years [1]–[4]. In the United States, for example, SuperPower Inc. has scaled up the length of YBCO CC [1], and then has succeeded in fabricating 1311 m long CC with the minimum critical current of 153 A/cm [2]. In Japan, on the other hand, GdBCO CC has also been researched and developed as a national project [3], and this has finally resulted in very large end-to-end critical current of 350 A/cm for 504 m long CC [4].

As is well known, significant advantages of CCs are very good transport properties against magnetic field thanks to REBCO materials and very high mechanical strength based on the substrates such as Hastelloy [5]. This means that the CCs can generate high magnetic field by a coil and can mechanically tolerate the corresponding electromagnetic force. Therefore, CCs have been greatly expected to be utilized for high-field coil systems such as magnet, SMES and NMR [5]–[7].

However, the design of a high-field coil using CCs is a challenging problem because we must consider too much about their current density versus electric field $(J-E)$ characteristics. The first is their temperature dependence. The coil will have temperature distribution in diverse ways depending on the relationship between the heat generation and the cooling condition. Thus, we should consider its influence on the current capacity of the coil. The second is magnetic field vector dependence. CCs have many kinds of pinning center (PC), and this brings relatively complicated dependence on magnetic field angle [8]. Therefore, we must carefully characterize such magnetic anisotropy for the coil design. The last is mechanical strain dependence. As for high-field coil, large stress and strain are applied to the conductor by electromagnetic force. On the other hand, $J-E$ characteristics in CCs are influenced by the strain although the CCs can reversibly tolerate such large strain. [9]–[12]. Hence, we should also discuss its influence on the transport performance of the coil.

Given this factor, we have characterized $J-E$ properties in a REBCO CC as a function of temperature, magnetic field vector, mechanical strain, and then have developed a thermally-electromagnetically-structurally coupled analysis code for a high-field magnet coil. In this paper, the $J-E$ properties are characterized for a GdBCO CC with critical current of 350 A/cm, and the coupled analysis is carried out for a design example of a 40 T class magnet coil using the CC.

Manuscript received August 26, 2008. First published June 05, 2009; current version published July 15, 2009. This work was supported in part by the "New Energy and Industrial Technology Development Organization (NEDO) as the Project for Development of Materials & Power Application of Coated Conductors, M-PACC", "JSPS: KAKENHI (20360143)" and "JSPS: KAKENHI (20.01945)."

K. Higashikawa, T. Kiss, M. Inoue and K. Imamura are with the Department of Electrical and Electronic Systems Engineering, Graduate School of Information Science and Electrical Engineering, Kyushu University, 744 Motooka, Nishi-Ku, Fukuoka 819-0395, Japan (e-mail: kohei@super.ees.kyushu-u.ac.jp; kiss@sc.kyushu-u.ac.jp; inoue@ees.kyushu-u.ac.jp; imamura@sc.kyushu-u.ac.jp).

T. Nakamura is with the Department of Electrical Engineering, Graduate School of Engineering, Kyoto University, Kyoto 615-8510, Japan (e-mail: tk_naka@kuee.kyoto-u.ac.jp).

S. Awaji and K. Watanabe are with the High Field Laboratory for Superconducting Materials, Institute for Materials Research, Tohoku University, Sendai 980-8577, Japan (e-mail: awaji@imr.tohoku.ac.jp; kwata@imr.tohoku.ac.jp).

H. Fukushima, Y. Yamada and Y. Shiohara are with the Superconductivity Research Laboratory, ISTEC, Tokyo 135-0062, Japan (e-mail: h-fukushima@istec.or.jp; htscrc01na@istec.or.jp; shiohara@istec.or.jp).

Color versions of one or more of the figures in this paper are available online at http://ieeexplore.ieee.org.

Digital Object Identifier 10.1109/TASC.2009.2018272

II. Analysis Method

A. $J-E$ Expressions for Coated Conductor

Nonlinear current transport characteristics in HTS materials are well understood by percolation transition model [13]. In particular, their $J-E$ characteristics are given by the following expressions using the minimum value, $J_{\rm cm}$, the half value of width, J_0, and a parameter representing the shape, m, of local critical current density distribution [14]–[18]:

$$J=\begin{cases} J_{\rm cm}+\left(\frac{m+1}{\rho_{\rm FF}}EJ_0^m\right)^{\frac{1}{m+1}} & \text{for } J_{\rm cm}\geq 0\ \mathrm{Am}^{-2} \\ -|J_{\rm cm}| & \\ \quad +\left(\frac{m+1}{\rho_{\rm FF}}EJ_0^m+|J_{\rm cm}|^{m+1}\right)^{\frac{1}{m+1}} & \text{for } J_{\rm cm}<0\ \mathrm{Am}^{-2} \end{cases} \tag{1}$$

where $\rho_{\rm FF}$ is resistivity at uniform flux flow. On the other hand, the minimum strength of pinning force density, $F_{\rm pm}=J_{\rm cm}B$, can be expressed as follows using the scaling function with glass-liquid transition magnetic flux density, $B_{\rm GL}$ [15]–[18]:

$$F_{\rm pm}(B)=J_{\rm cm}(B)B=AB_{\rm GL}^{\zeta}\left(\frac{B}{B_{\rm GL}}\right)^{\gamma}\left(1-\frac{B}{B_{\rm GL}}\right)^{\delta} \tag{2}$$

where A, ζ, γ and δ are pin parameters. $F_{\rm pk}=(J_{\rm cm}+J_0)B$ is also given by the same form as (2). Furthermore, temperature dependence of $B_{\rm GL}$ can be expressed by the following expression [16]–[18]:

$$B_{\rm GL}(T)=\frac{b}{1-\nu_{\rm p}}\left(1-\frac{T}{T_{\rm c}}\right) \times\left(1-\frac{a}{1-\frac{T}{T_{\rm c}}}+\sqrt{\left(1+\frac{a}{1-\frac{T}{T_{\rm c}}}\right)^2-4\nu_{\rm p}\frac{a}{1-\frac{T}{T_{\rm c}}}}\right) \tag{3}$$

where a, b and $\nu_{\rm p}$ are numerical parameters. By introducing (2) and (3) into (1), we can obtain the $J-E$ characteristics as a function of temperature, T, and magnetic field, B.

On the other hand, especially for CCs, the parameters' values are different depending on the applied angle of magnetic field because the corresponding dominant PC is also different [18]. In this study, we consider three kinds of PCs, i.e., ab-plane-correlated PC, random point PC and c-axis-correlated PC, in order to describe the $J-E$ characteristics also as a function of the magnetic field angle, θ. Fig. 1 shows a typical comparison of critical current density, $J_{\rm c}$, versus θ between the analytical expressions and experimental data obtained for the GdBCO CC. The value of $J_{\rm c}$ is defined for the GdBCO layer with the thickness of 1.2 μm. As shown in the figure, the expressions can describe the experimental data very well at 65 K and 20 K, and also can predict the data at 4 K (the experimental data at 4 K includes large error in θ because of the failure of rotating machinery for the sample). We will report the detailed formulation of this separately.

In addition, in order to consider the influence on mechanical strain, ε, on the $J-E$ characteristics, we introduce the following expression which has already been proposed by J. W. Ekin for effective upper magnetic field of a Nb_3Sn conductor [19]:

$$B_{\rm GL}(\varepsilon)=\left(1-\alpha|\varepsilon-\varepsilon_{\rm m}|^{\upsilon}\right)B_{\rm GL}(\varepsilon_{\rm m}) \tag{4}$$

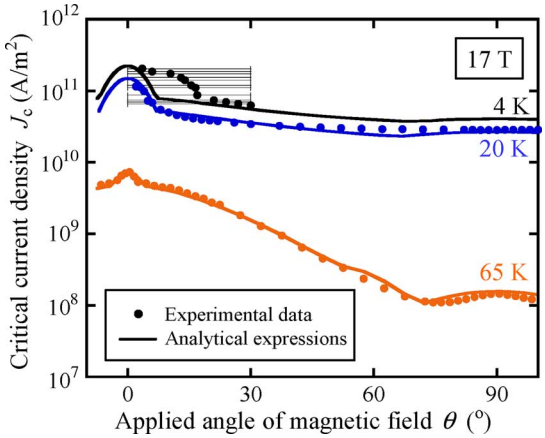

Fig. 1. Comparison of critical current density versus applied angle of magnetic field characteristics between experimental data and analytical expressions obtained for a GdBCO CC. The critical current density is defined for the GdBCO layer with the thickness of 1.2 μm. The experimental data at 4 K includes large error in angle due to a temporary failure of rotating machinery.

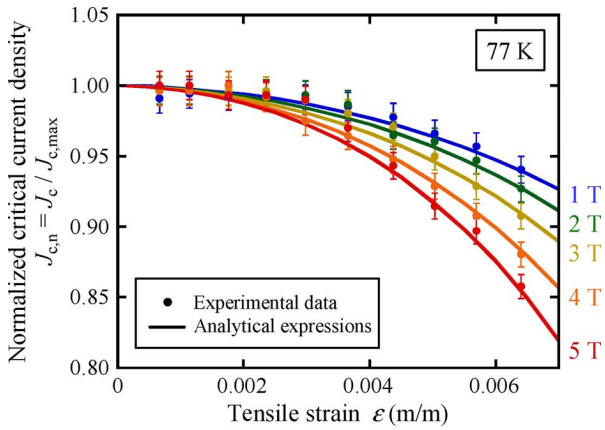

Fig. 2. Comparison of normalized critical current density versus applied tensile strain characteristics between experimental data and analytical expressions obtained for a GdBCO CC at 77 K.

where α and υ are numerical parameters, and $\varepsilon_{\rm m}$ is a correction value to compensate ε for the conductor to intrinsic strain for the superconducting material, $\varepsilon_0=\varepsilon-\varepsilon_{\rm m}$. Fig. 2 shows a comparison of axial strain dependence on critical current density normalized by its maximum value, $J_{\rm c,n}=J_{\rm c}/J_{\rm c,max}$, between the analytical expressions and experimental data obtained for a GdBCO CC. As shown in the figure, the strain dependence can be described very well. We will report the details about the experimental systems, the results and the formulation elsewhere.

Using these formulations, the current transport properties in REBCO CC are given as a function of temperature, magnetic field, its angle and mechanical strain: $J(E,T,B,\theta,\varepsilon)$.

B. Coupled Analysis Code for High-Field Magnet Coil

Fig. 3 shows the conceptual diagram of the thermally-electromagnetically-structurally coupled analysis code for a high-field magnet coil. The analysis code is composed of three modules. The first is an electromagnetic analysis module. The $J(E,T,B,\theta,\varepsilon)$ characteristics in the CC are introduced into this module. The second is a thermal analysis module. The

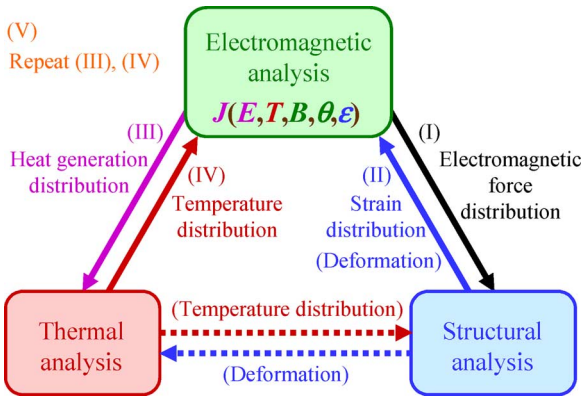

Fig. 3. Conceptual diagram of a thermally-electromagnetically-structurally coupled analysis code for a high-field magnet coil. The parenthetic items are not considered for the results shown in this paper.

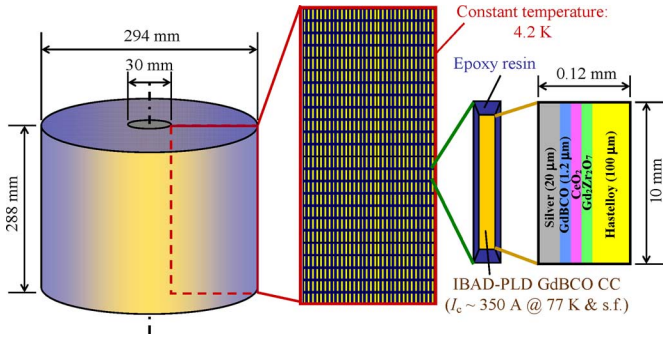

Fig. 4. Illustration of a design example of a 40 T class coil to be analyzed. An IBAD-PLD GdBCO CC with critical current of 350 A at 77 K and self-field is supposed to be used for the winding, which is impregnated with epoxy resin. The corresponding volume ration of the CC is 50%.

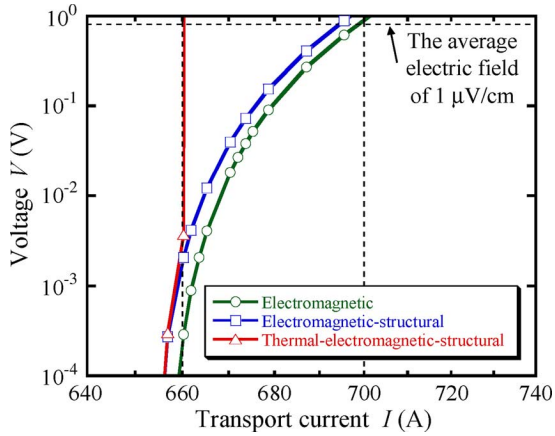

Fig. 5. Analysis results on transport current versus voltage characteristics of the coil. The characteristics are obtained by means of three kinds of analysis procedure. The horizontal axis as well as the vertical axis is logarithmic scale.

third is a structural analysis module. Each of the three modules employs finite element method (FEM).

In this paper, only the steady state is discussed, and the analysis are carried out only in the conditions where the parenthetic items in Fig. 3 can be neglected The corresponding analysis procedure for each value of transport current, I, can be described as follows:

(I): Electromagnetic analysis calculates the distribution of electromagnetic force in the coil. Uniform distributions of temperature and strain are assumed here: $T = T_{\rm op}$ and $\varepsilon = 0$ for every element where $T_{\rm op}$ is operating temperature.

(II): Structural analysis estimates the deformation of the coil. The corresponding strain distribution is fed back to the electromagnetic analysis.

(III): Electromagnetic analysis recalculates the distribution of heat generation in the coil.

(IV): Thermal analysis calculates the distributions of temperature in the coil. The obtained temperature distribution is fed back to the electromagnetic analysis.

(V): Items (III) and (IV) are repeated until the convergence. However, the calculation is also stopped when the maximum temperature in the coil, $T_{\rm max}$, exceeds critical temperature of the conductor, $T_{\rm c}$. This means quench will occur in such operating conditions. I and $T_{\rm op}$.

C. Example of GdBCO Coil for Coupled Analysis

Fig. 4 illustrates an example of a GdBCO coil to be analyzed. A GdBCO CC with critical current of 350 A fabricated by IBAD-PLD process is supposed to be used for the winding. The width of the CC is 10 mm, and the thickness is 0.12 mm including 100 μm of Hastelloy, 1.2 μm of GdBCO and 20 μm of silver layers. The winding is impregnated with epoxy resin, and the corresponding volume ratio of the CC is 50%. The inside diameter, the outside diameter and the height of the coil are optimized *only by electromagnetic analysis* under the following constraint conditions:

- The maximum magnetic field generated by the coil, $B_{\rm max}$, is 40.0 T.
- Operating temperature is 4.2 K on the assumption of liquid helium cooling.
- Transport current does not exceed critical current, $I_{\rm c}$, everywhere in the coil. In other words, the maximum electric field in the coil, $E_{\rm max}$, is not larger than the electric field criterion, $E_{\rm c} = 1.0 \times 10^{-4}\ {\rm V/m} (= 1.0\ \mu{\rm V/cm})$.
- Hoop tensile force applied to one turn of the coil, $F_{\rm h}$, does not exceed 1.0 kN everywhere in the coil. It has been reported that a CC with Hastelloy substrate can reversibly tolerate such large tensile force [12]. The corresponding tensile strain is roughly estimated to be 0.5%.
- Lower limit of the inside diameter is set to be 30 mm according to past achievements of a small coil using the CC [20], [21].

III. Results and Discussion

Fig. 5 shows the analysis results on transport current versus voltage, V, characteristics of the coil. The characteristics are obtained by means of three kinds of analysis procedure. The first is electromagnetic analysis only (just item (I) is executed). The second is electromagnetically-structurally coupled analysis where influences of the strain distribution on the characteristics are considered (items (I)–(III) are carried out). The third is thermally-electromagnetically-structurally coupled analysis where

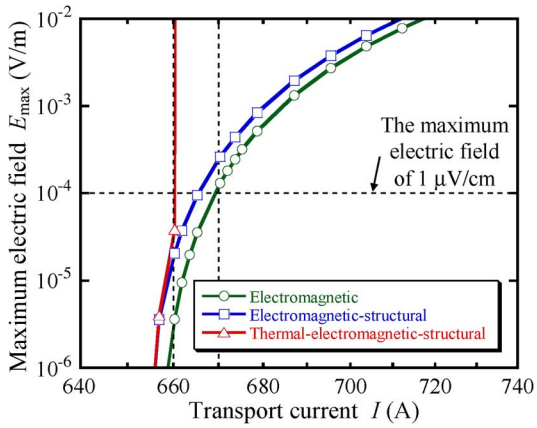

Fig. 6. Analysis results on transport current versus the maximum electric field characteristics in the coil. The horizontal axis as well as the vertical axis is logarithmic scale.

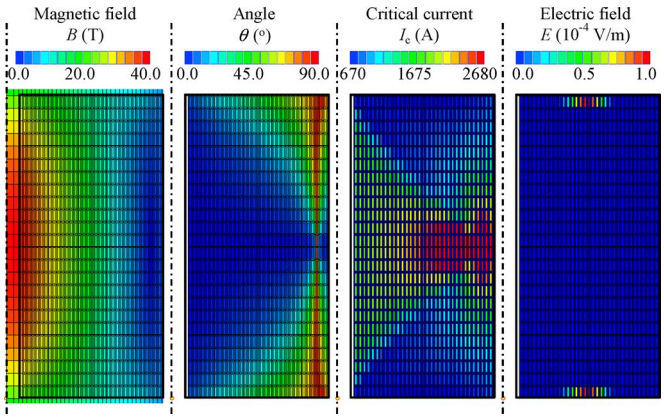

Fig. 7. Electromagnetic analysis results on the distributions of magnetic field, its angle, critical current and electric field at the transport current of 670 A.

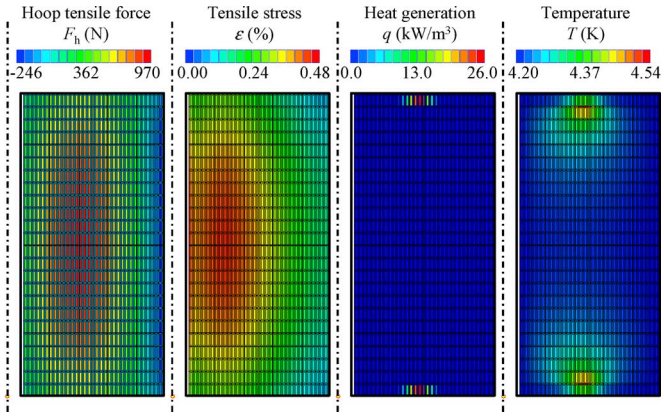

Fig. 8. Coupled analysis results on the distributions of hoop tensile force, tensile stress, heat generation and temperature at the transport current of 660 A.

influences also of the temperature distribution are taken into account (items (I)–(V) are completed). Fig. 6 also shows the corresponding results on transport current versus the maximum electric field characteristics in the coil.

A. 40 T Coil Designed Only by Electromagnetic Analysis

The shape of the $I - V$ characteristics obtained only by electromagnetic analysis is convex upward on the double logarithmic plot, and this kind of the shape is well known for $J - E$ characteristics of HTS materials in glass state [13]. The broken line indicating $V = 0.81$ V in Fig. 5 means that the average electric field of the coil, E_{ave}, is equal to the criterion $E_c = 1.0 \times 10^{-4}$ V/m because the total length of the CC used for the coil is 8.1 km. Such a criterion is often used for the definition of the critical current of HTS coils because it is relatively convenient only to monitor their terminal voltage. In this analysis, the corresponding transport current is 700 A. However, as shown in Fig. 6, E_{max} is estimated to be 30 times larger than E_c for such transport current. On the other hand, $I = 670$ A is estimated for $E_{max} = E_c$, and this is the design point of the coil for the generation of $B_{max} = 40.0$ T.

Fig. 7 shows the detailed results on the coil at the design point. The $B_{max} = 40.0$ T is generated inside the bore near the innermost layer of the coil. The region of large I_c is spread in that of small θ (almost parallel to the broad surface of the CC) as well as in that of low B. In particular, I_c is large for $\theta < 5°$ almost independently of B. This can be recognized as an effect of strong flux pinning by *ab*-plane correlated PC (see Fig. 1). In contrast, the minimum value of I_c, $I_{c,mn}$ is located near the middle layer on the top and bottom edges in the coil. The $I_{c,mn} = 670$ A is determined by $B = 14.4$ T and $\theta = 38.0°$. These are the results at the designed point only by electromagnetic analysis.

B. 40 T Coil Analyzed by Coupled Analysis Code

However, as shown in Figs. 5 and 6, it has been suggested from the thermally-electromagnetically-structurally coupled analysis that the coil cannot keep superconducting state for such a designed transport current of 670 A. In this case, $I = 660$ A is estimated as the maximum current capacity of the coil although E_{max} is still smaller than E_c.

Fig. 8 shows of the detailed results of the coupled analysis at the $I = 660$ A. For this transport current, $E_{max} = 3.6 \times 10^{-6}$ V/m is estimated only by electromagnetic analysis. On the other hand, tensile strain is induced in the coil as shown in the figure. The distribution of the strain is slightly different from that of hoop tensile force (which is given by the product of magnetic field parallel to the coil's axis, transport current and bending radius, r [22]). If each turn of the coil can move freely, the distribution of the two should be the same. However, structural analysis can consider the interaction between adjacent turns. Then, inner turn tends to move with outer turn in radial direction. If the displacement in the radial direction, Δr, is the same, larger strain is induced in the turn with smaller r because the tensile strain is given by $\Delta r/r$. Accordingly, the region of large tensile strain is shifted inward compared with that of hoop tensile force. Anyway, the maximum strain is 0.48%, and this can be reversibly tolerated by the CC. However, lager $E_{max} = 2.1 \times 10^{-5}$ V/m is estimated due to the strain. Furthermore, such electric field means the existence of heat generation. As a result, temperature rises from 4.20 K to 4.54 K, and then balances at even larger $E_{max} = 3.9 \times 10^{-5}$ V/m. These are the coupled analysis results obtained at $I = 660$ A.

On the other hand, if the transport current is larger than 660 A, such vicious circle of increasing temperature and electric field does not permit the coil to be stabilized in superconducting state.

Therefore, the maximum current capacity of the coil is estimated to be 660 A although the designed value of the transport current is 670 A for $B_{\max} = 40.0$ T. It should be noted that such a difference can be obtained even though the analysis is carried out for relatively ideal conditions: liquid helium cooling and perfect impregnation with epoxy resin. This strongly indicates that the influences of temperature rise and mechanical strain in the coil should be taken into account for the design of high-field magnet coils. Furthermore, additional mechanical strain will be applied to the CC at the stages of coil winding at room temperature and cooling down to 4.2 K. We believe that we will also be able to understand such influences by improving this coupled analysis method.

IV. Conclusion

We have characterized current transport properties of a GdBCO CC as a function of temperature, magnetic field vector and mechanical strain, and then have carried out a thermally-electromagnetically-structurally coupled analysis for a design example of a 40 T class coil. We have shown the influences of temperature rise and mechanical strain on the transport performance of the coil, and have indicated the necessity of the consideration of such influences for the design of high-field magnet coils using CCs.

References

[1] V. Selvamanickam, Y. Chen, X. Xiong, Y. Xie, X. Zhang, Y. Qiao, J. Reeves, A. Rar, R. Schmidt, and K. Lenseth, "Progress in scale-up of second-generation HTS conductor," *Physica C*, vol. 463–465, pp. 482–487, 2007.

[2] SuperPower Inc., August 6, 2008, Press Releases [Online]. Available: http://www.superpower-inc.com/news.php?n=157

[3] Y. Shiohara, M. Yoshizumi, T. Izumi, and Y. Yamada, "Present status and future prospect of coated conductor development and its application in Japan," *Supercond. Sci. Technol.*, vol. 21, no. 3, p. 034002, 2008.

[4] Fujikura Ltd., May 14, 2008, News Release [Online]. Available: http://www.fujikura.co.jp/newsrelease/1190219_2220.html

[5] J. Schwartz, T. Effio, L. Xiaotao, Q. V. Le, A. L. Mbaruku, H. J. Schneider-Muntau, T. Shen, H. Song, U. P. Trociewitz, X. Wang, and H. W. Weijers, "High field superconducting solenoids via high temperature superconductors," *IEEE Trans. Appl. Supercond.*, vol. 18, no. 2, pp. 70–81, 2008.

[6] K. Higashikawa, T. Nakamura, K. Shikimachi, N. Hirano, S. Nagaya, T. Kiss, and M. Inoue, "Conceptual design of HTS coil for SMES using YBCO coated conductor," *IEEE Trans. Appl. Supercond.*, vol. 17, no. 2, pp. 1990–1993, 2007.

[7] K. Higashikawa, T. Nakamura, M. Sugano, K. Shikimachi, N. Hirano, and S. Nagaya, "Performance improvement of YBCO coil for high-field HTS-SMES based on homogenized distribution of magnetically-mechanically influenced critical current," *IEEE Trans. Appl. Supercond.*, vol. 18, no. 2, pp. 758–761, 2008.

[8] L. Civale, B. Maiorov, A. Serquis, J. O. Willis, J. Y. Coulter, H. Wang, Q. X. Jia, P. N. Arendt, J. L. MacManus-Driscoll, M. P. Maley, and S. R. Foltyn, "Angular-dependent vortex pinning mechanisms in $YBa_2Cu_3O_7$ coated conductors and thin films," *Applied Physics Letters*, vol. 84, no. 12, pp. 2121–2123, 2004.

[9] N. Cheggour, J. W. Ekin, C. L. H. Thieme, Y.-Y. Xie, V. Selvamanickam, and R. Feenstra, "Reversible axial-strain effect in Y-Ba-Cu-O coated conductors," *Supercond. Sci. Technol.*, vol. 18, pp. S319–S324, 2005.

[10] N. Cheggour, J. W. Ekin, and C. L. H. Thieme, "Magnetic-field dependence of the reversible axial-strain effect in Y-Ba-Cu-O coated conductors," *IEEE Trans. Appl. Supercond.*, vol. 15, no. 2, pp. 3577–3560, 2005.

[11] D. Uglietti, B. Seeber, V. Abächerli, W. L. Carter, and R. Flükiger, "Critical currents versus applied strain for industrial Y-123 coated conductors at various temperatures and magnetic fields up to 19 T," *Supercond. Sci. Technol.*, vol. 19, pp. 869–872, 2006.

[12] M. Sugano, T. Nakamura, K. Shikimachi, N. Hirano, and S. Nagaya, "Stress tolerance and fracture mechanism of solder joint of YBCO coated conductor," *IEEE Trans. Appl. Supercond.*, vol. 17, no. 2, pp. 3067–3070, 2007.

[13] K. Yamafuji and T. Kiss, "Current-voltage characteristics near the glass-liquid transition in high- T_c superconductors," *Physica C*, vol. 213, pp. 9–22, 1997.

[14] T. Kiss, T. Nakamura, N. Mishiro, K. Hasegawa, M. Inoue, M. Takeo, F. Irie, and K. Yamafuji, "Transport characteristics in high T_c superconductors," in *Proc. MT15*, 1998, no. 2, pp. 1052–1055.

[15] T. Kiss, K. Hasegawa, M. Inoue, M. Takeo, H. Okamoto, and F. Irie, "Critical current properties in high T_c superconductors," (in Japanese) *Cryogenic Engineering (Teion-Kogaku)*, vol. 34, no. 7, pp. 322–331, 1999.

[16] T. Kiss, M. Inoue, T. Kuga, M. Ishimaru, S. Egashira, S. Irie, T. Ohta, K. Imamura, M. Yasunaga, M. Takeo, T. Matsushita, Y. Iijima, K. Kakimoto, T. Saitoh, S. Awaji, K. Watanabe, and Y. Shiohara, "Critical current properties in HTS tapes," *Physica C*, vol. 392–396, pp. 1053–1062, 2003.

[17] M. Inoue, T. Kiss, T. Kuga, M. Ishimaru, M. Takeo, T. Matsushita, Y. Iijima, K. Kakimoto, T. Saitoh, S. Awaji, K. Watanabe, and Y. Shiohara, "Critical current properties of a YBCO coated conductor in high magnetic fields," (in Japanese) *IEEJ Trans. Fundamentals and Materials*, vol. 123, no. 6, pp. 593–599, 2003.

[18] M. Inoue, T. Kiss, D. Mitsui, T. Nakamura, T. Fujiwara, S. Awaji, K. Watanabe, A. Ibi, S. Miyata, Y. Yamada, and Y. Shiohara, "Current transport properties of 200 A—200 m—Class IBAD YBCO coated conductor over wide range of magnetic field and temperature," *IEEE Trans. Appl. Supercond.*, vol. 17, no. 2, pp. 3207–3210, 2007.

[19] J. W. Ekin, "Strain scaling law for flux pinning in practical superconductors. Part 1: Basic relationship and application to Nb_3Sn conductors," *Cryogenics*, vol. 20, no. 11, pp. 611–624, 1980.

[20] H. Fukushima, A. Ibi, H. Takahashi, R. Kuriki, S. Miyata, Y. Yamada, Y. Shiohara, T. Kato, and T. Hirayama, "Properties of long GdBCO coated conductor by IBAD-PLD method—The first GdBCO coil test," *IEEE Trans. Appl. Supercond.*, vol. 17, no. 2, pp. 3367–3370, 2007.

[21] H. Fukushima, A. Ibi, H. Takahashi, R. Kuriki, S. Miyata, Y. Yamada, and Y. Shiohara, "GdBCO and YBCO long coated conductors and coils," *Physica C*, vol. 463–465, pp. 501–504, 2007.

[22] A. Otsuka and T. Kiyoshi, "High-field magnet design under constant hoop stress," *IEEE Trans. Appl. Supercond.*, vol. 18, no. 2, pp. 1529–1532, 2008.